Title

ANGLE-RESOLVED PHOTOEMISSION STUDIES OF TH VALENCE-BAND STRUCTURE OF STEPPED CRYSTAL SURFACES: Cu(S)-[3(lll)x(100)l

Author

Davis, R.F.

Publication Date

1984-09-01

Lawrence Berkeley Laboratory
UNIVERSITY OF CALIFORNIA

Materials & Molecular Research Division

Submitted to Physical Review B

ANGLE-RESOLVED PHOTOEMISSION STUDIES OF THE VALENCE-BAND STRUCTURE OF STEPPED CRYSTAL SURFACES: Cu(S)-[3(111)x(100)]

R.F. Davis, R.S. Williams, S.D. Kevan,
P.S. Wehner and D.A. Shirley

September 1984

Prepared for the U.S. Department of Energy under Contract DE-AC03-76SF00098

DISCLAIMER

LBL-8511 Rev.

ANGLE-RESOLVED PHOTOEMISSION STUDIES OF THE VALENCE-BAND STRUCTURE OF STEPPED CRYSTAL SURFACES: Cu(S)-[3(111)x(100)]

R. F. Davis, R. S. Williams, S. D. Kevan,
P. S. Wehner, and D. A. Shirley

Materials and Molecular Research Division
Lawrence Berkeley Laboratory
and
Department of Chemistry
University of California
Berkeley, California 94720

September 1984

ANGLE-RESOLVED PHOTOEMISSION STUDIES OF THE VALENCE-BAND STRUCTURE OF STEPPED CRYSTAL SURFACES: Cu(S)-[3(111)x(100)]

R. F. Davis,* R. S. Williams,† S. D. Kevan,‡
P. S. Wehner,§ and D. A. Shirley

Materials and Molecular Research Division
Lawrence Berkeley Laboratory
and
Department of Chemistry
University of California
Berkeley, CA 94720

ABSTRACT

Angle-resolved photoemission spectra are reported for the stepped Cu(211) face in the photon-energy range 9 eV $\leq h\nu \leq$ 34 eV. The valence-band (VB) spectra are interpreted in terms of a direct-transition model for bulk photoemission. Determination of VB dispersion relations and assignment of the bands are aided by use of selection rules involving the transmitted radiation vector potential and several different experimental geometries. The major results are: (1) it is possible to determine experimental VB dispersion relations for a lower-symmetry direction such as Cu[211] and (2) VB dispersion relations for stepped Cu(211) show excellent agreement with bulk valence bands interpolated along the [211] direction, uninterrupted

---

*Present address: Polaroid Corporation, Waltham, MA 02154
†Present address: Department of Chemistry & Biochemistry, University of California, Los Angeles, CA 90024 - Camille & Henry Dreyfus Teacher-Scholar and Alfred P. Sloan Fellow.
‡Present address: Bell Laboratories, Murray Hill, NJ 07974.
§Present address: Tennessee Eastman Company, Kingsport, TN 37662.

by band-gap photoemission, the effects of which are not observed. It is concluded that the unusual structure of the stepped surface does not significantly perturb the bulk electronic structure near the surface in this case.

I. INTRODUCTION

Detailed angle-resolved photoemission (ARP) studies of the face-centered cubic (FCC) metals copper,[1-5] silver,[6,7] gold,[8-11] nickel,[12] palladium,[13] platinum,[8,14] and iridium[15] have shown that the peak structures in photoelectron energy distribution curves (EDCs) arise mainly from energy- and crystal momentum-conserving direct electronic transitions near or at the surface. Consequently, by combining the photon-energy variability of synchrotron radiation with a normal electron-emission geometry, these studies[1,2,4,6,8,9,12-15] have resulted in the determination empirical bulk valence-band dispersion relations along $\vec{k}_\perp$ (the surface perpendicular or normal component of the crystal momentum $\vec{k}$) with remarkable success. However, in each case, the surface studied was a low-Miller-index plane [i.e., (100), (110), or (111)]. These studies yielded experimental energy bands along high-symmetry lines in k-space, permitting ready comparisons to published theoretical band-structure calculations.

In this paper, we report angle-resolved normal photoemission (ARNP) valence-band studies of the Cu(211) face, a Cu(S)-[3(111)x(100)] stepped surface, of which an ideal segment is depicted in Fig. 1. These experiments address directly a number of important problems in photoemission from metals. The complexity of ARNP from (110) and (100) faces[16] relative to (111) suggests that a detailed understanding of ARNP from still lower symmetry faces -- such as (211) -- might be very difficult. This hypothesis has several

origins. First, low k-space symmetry completely lifts the degeneracy of the energy bands along much of the [211] line. Second, the relatively large surface unit cell of a high-index face gives rise to a set of small two-dimensional reciprocal lattice vectors, which may induce surface Umklapp of photoelectrons with higher cross section than that on unreconstructed low-index faces.[17] Furthermore, like many high-index faces of the Group VIII and I-B metals oriented in the $[0\bar{1}1]$ crystallographic zone,[18] the clean Cu(211) surface develops a stable stepped structure after annealing. The electronic structure of stepped and kinked surfaces is of considerable interest because the step and/or kink atoms on such surfaces are believed to influence surface reactivity.[19] Although there is some experimental[20] and theoretical[21] evidence that enhancement of surface reactivity may arise more from steric effects due to step-adsorbate geometry than from any particular electronic-structural property of the steps, some theoretical calculations predict, in certain cases, substantially different electronic environments for step or kink atoms relative to atoms on planar surfaces.[22,23]

A detailed understanding of the photoemission process from Cu(211) is obtained simply within the framework of the direct-transition model using a quasi-free electron final-state band structure. Furthermore, although the low symmetry of Cu(211) does indeed introduce a great deal of structure of the EDCs, it also enables us to investigate the symmetry and dispersion properties of each individual valence band.

In Section II, we discuss experimental procedures. Section III

describes the results within a bulk direct-transition framework, and Section IV summarizes our study.

II. EXPERIMENTAL PROCEDURE

A high purity single crystal slab of Cu was cut and mechanically polished to within ±0.5° of the (211) plane (19.5° from [111] in the [01$\bar{1}$] zone), with a mean surface roughness of 1-μm. After a chemical polish,[26] the crystal was installed in an ultrahigh-vacuum chamber (base pressure ~3 x 10^{10} torr) for *in situ* preparation and characterization.[18,27] Preparation was accomplished by repeated cycles of Ar^+ sputtering, followed by annealing at ~875K. Immediately preceding the ARP experiments, the resulting surface was monitored by Auger electron spectroscopy (AES) for cleanliness and low energy electron diffraction (LEED) for crystallographic order, giving rise to AES impurity signals characteristic of ≲0.05 monolayer contamination and LEED patterns (with extremely sharp and intense spots) characteristic of the stable step surface structure. As shown in Fig. 1, the (211) surface consists of (111) oriented terraces with three inequivalent atomic rows (labeled A, B, and C) that are parallel to the [01$\bar{1}$] direction, and monatomic steps of (100) orientation. The only symmetry element that this surface contains is the (01$\bar{1}$) mirror plane which cuts through the surface perpendicular to the atomic rows.

The photoemission measurements were performed on the 8° branch of Beam Line I (BL I-2) at the Stanford Synchrotron Radiation Laboratory. The incident radiation was highly polarized (> 97%) in the

horizontal plane and in the energy range 9 eV $\leq h\nu \leq$ 34 eV. Our ARP instrument, described elsewhere,[28] employs a rotatable 5.40 cm mean radius hemispherical analyzer with an angular acceptance of ±3°. In these measurements, the energy resolution (monochromator plus electron analyzer) varied from ca. 0.12 eV to ca. 0.25 eV (FWHM) at the lower and upper photon energies, respectively.

As shown in Fig. 2, experiments were done with two different normal emission geometries, conversion between which was achieved by azimuthal rotation of the crystal about its normal ($\vec{n}$) by 90°. For both orientations, the incident radiation vector potential ($\vec{A}$) was confined to the plane of incidence, and the photoemission direction ($\vec{p}$) was confined to the surface normal ([211]). In orientation I [Fig. 2(a)], $\vec{A}$ lies in a crystallographic plane perpendicular to the $(01\bar{1})$ mirror plane (M) with $\phi_A = 0°$, whereas in orientation II [Fig. 2(b)], $\vec{A}$ lies in M (M is the plane of incidence in this case) with $\phi_A = 270°$. The angle θ_A (between $\vec{n}$ and $\vec{A}$) could be varied between 10° and 45° in either θ_A azimuth by coupling analyzer and crystal polar rotations, but the majority of measurements were performed with $\theta_A = 30°$. At this angle, $\vec{A}$ is aligned with the [110] direction in orientation I, and is ~ 5° from alignment with [100] in orientation II. <u>In situ</u> polar crystallographic alignment (± 1°) was achieved using a He-Ne laser, and the azimuthal orientation (± 3°) was determined from LEED patterns. We shall henceforth refer to the above sample orientations simply as (I) and (II).

Typical EDCs for the entire energy range are shown in Fig. 3 for

both orientations and $\theta_A = 30^\circ$. Only 24 spectra are plotted here, for brevity. Our interpretation is based on a total of 82 spectra. In each spectrum, the Fermi level (E_F) was determined as $(dJ/dE)_{max.}$, i.e., the point of maximum derivative of photoelectron intensity with respect to energy, in the region near the onset of the s-p plateau. Because of relatively low intensity (J), this procedure became progressively more difficult in the higher photon-energy region ($h\nu \gtrsim 20$ eV), particularly for the spectra taken with the sample in (I). Nevertheless, the work functions derived from E_F placement and analyzer reference voltages showed an rms scatter of only ± 35 meV for the entire data set.

III. RESULTS AND DISCUSSION

The spectra shown in Fig. 3 clearly indicate that (a) the low symmetry of the (211) face introduces complexity to the valence-band peak structure relative to the spectra of low-index Cu faces, and (b) there is a strong dependence on radiation polarization, as the only difference between the two orientations is the direction of $\vec{A}$ relative to the crystallographic axes. The behavior of the various contributions to the spectra, which can be identified and shown to disperse with photon energy, is highly indicative of bulk direct-transition processes, particularly because $\vec{k}_{\parallel}$ (surface component of momentum) is zero for normal emission. This behavior is demonstrated by the structure plots for both orientations, shown in Fig. 4. The circles represent strong peak (closed circles) or weak feature (open

circles) energy positions relative to E_F for the range of photon energies used. The connecting lines on the plots in Fig. 4 have no significance other than to join and map the individual structures as a function of $h\nu$. The reproducibility between the two sets of plots [(I) and (II)] is excellent: the derived energies of equivalent peaks which are found in spectra for both orientations (at a given $h\nu$) typically agree within 0.04 eV or less. The bands are labeled according to a notation to be described below.

In the normal emission geometry, peak energy dispersion with $h\nu$ as shown in Fig. 4 can only occur from direct transitions at reduced k-points that yield photocurrent in normal emission, i.e., k-points that either are part of the [211] direction crystal momentum space (primary Mahan cones[29]), or are in other directions but can excite transitions that result in normal emission via surface Umklapp processes (secondary cones[17,24]). We proceed below to set up a bulk band-structure framework[30] with which to interpret the data represented in Figs. 3 and 4, and we show that excellent agreement between experiment and theory is obtained if (a) only $\vec{k}_\perp$-conserving transitions from [211] initial states are assumed to occur, and (b) only one final state band is important in transmitting photocurrent to the analyzer (i.e., no secondary Mahan cones contribute <u>peak</u> structures).

The irreducible portion of k-space lying along [211], all of which is contained in the $(01\bar{1})$ plane, is shown as the dashed line in Fig. 5. The point B = (3/4,3/8,3/8) (in units of $2\pi/a$, which will be

used throughout this work) is equivalent to D = (-1/4,-5/8,-5/8), both being at the Brillouin zone boundary. Although these points have no other significance or special symmetry properties, it is useful to designate them as B and D. The group of the $\vec{k}$-vector (the point group C_s) corresponding to points along [211] ($\Gamma \rightarrow B$, $D \rightarrow X$) contains only the identity element (E) and the $(01\bar{1})$ mirror plane (σ_h). Thus, electronic states lying on the [211] crystal momentum axis may be symmetry classified as either even or odd (A' or A", respectively, in C_s) with respect to reflection through the mirror plane.

The energy bands for Cu were generated for the [211] crystal momentum line, using Smith's band-structure interpolation scheme, which utilizes a mixed basis set consisting of five atomic d-orbitals and sixteen plane waves[31] and is an extension of the Hodges, Ehrenreich, and Lang formalism.[32] The parameters used for the calculation were obtained in Ref. 31 by fitting to the energy bands of Janak, et al.,[33] stretching the valence band by 8% along the energy scale to agree with photoemission data. The agreement of the interpolated bands with the first-principles results of Janak, et al.,[33] and with those of Burdick[34] are quite good, even extending 20 eV above the Fermi level. The energy bands were generated along the [211] direction by folding the dashed lines shown in Fig. 5 into the irreducible $(^1/48)^{th}$ of the first Brillouin zone with $k_y \geq k_x \geq k_z \geq 0$, and diagonalizing the interpolation Hamiltonian for the resulting k-values.

From careful inspection of the eigenvectors in our calculation, we

determined the irreducible representations (A' or A") of the first eight bands at each k-point, and have labeled accordingly the bands shown in Fig. 6. We found it useful to label the bands of each type separately according to increasing band index, but this has no group-theoretical significance. It does, however, remove ambiguities caused by band crossings. Of the six valence bands, four have A' symmetry, while the two lowest conduction bands also have A' symmetry. As shown, the band structure reveals a gap in the conduction bands between A_5' and A_6' from about 10.8 eV to 12.0 eV above E_F, and a rather complex behavior beginning at 23.7 eV above E_F. In principle, a conduction-band gap has implications for ARP if it involves the photoemission final states.[17,24,25]

Hermanson[35] has discussed the polarization selection rules for photoemission normal to low-index faces of cubic crystals, and there have been several experimental studies of these polarization effects.[2,36] In this study, we have incorporated two different polarization geometries to investigate the importance of these effects for a stepped crystal face, for which the symmetry properties are simple. Polarization selection actually reduces considerably the problem of determining dispersion relations for each individual valence band in Cu(211), as will be discussed below. The selection rules governing ARNP from Cu(211) are summarized in Table I. The photoemission final state must belong to the A' (symmetric) irreducible representation because operations which leave the crystal invariant should not affect the electronic state sampled by the

detector. Thus, in order for a transition to be allowed, the irreducible representation of a particular initial state must be contained in the transition operator $\vec{A}\cdot\vec{p}$. Referring to Fig. 2 and Table I, the component of $\vec{A}$ along $[01\bar{1}]$ (orthogonal to M) can excite A" initial states (A_1" or A_2"), while components along [211] and $[\bar{1}11]$ (lying in M) excite only A' (A_1' through A_4') initial states. Thus, for the geometries shown in Fig. 2, the spectra accumulated in (I) may arise from A' → A' and A" → A' transitions. On the other hand, the spectra from (II), with $A_x = 0$, should arise from A' initial state bands only. Inspection of relative peak intensities in the spectra (Fig. 3) indicates a qualitative verification of these selection rules for Cu(211) direct transitions. Aided by direct comparison of interpolated and experimental band structures (see below), we have labeled the structure plots in Fig. 4 according to the initial states involved in the transitions.

In consonance with previous studies,[6,8,9,14] the photoemission final states were taken partly to be A' conduction-band components that are derived from the empty-lattice conduction band(s) that would be involved in [211] primary Mahan[29] cone emission. Between Γ and B, there are no unbound primary cone components for photoemission with $h\nu \leq 34$ eV, since the smallest reciprocal lattice vector involved in a primary cone transition $\vec{k}_i \rightarrow \vec{k}_i - \vec{G}$ (in the empty lattice approximation) would be $\vec{G} = (4,2,2)$; this would require $h\nu > 170$ eV at $\vec{k}_i$ = B. However, there is primary emission in our energy range from final states between D and X, shown in Fig. 6 as the regions of A_5'

and A_6' highlighted by cross hatches. These states are derived from $\vec{G} = (\bar{1},\bar{1},\bar{1})$. In the band-gap regions, 10.8 eV $\leq E^F \leq$ 12.0 eV and $E^F \geq$ 23.7 eV, the final states were derived from $E^F(\vec{k}) = (\hbar^2/2m^*)|\vec{k} - \vec{G}|^2 + V_0^F$, with $\vec{G} = (\bar{1},\bar{1},\bar{1})$. These states are shown in Fig. 6 as filled circles between A_5' and A_6' and extending beyond A_6'. The parameters m* (reduced mass) and V_0^F (inner potential) were calculated from a fit of this free-electron-like dispersion relation to the regions of A_5' and A_6', highlighted by cross hatches in Fig. 6, yielding $m^* = 0.89\ m_e$ and $V_0^F = -8.0$ eV. This value of m* is consistent with that determined experimentally by Knapp, et al.[2] for the Δ_1 conduction band in Cu(001) [$(m^*/m_e = 0.90$ to $0.94]$. Using the measured[37] value for the Cu(211) work function ($\Phi = 4.53$ eV), we obtain $V_0^V = -12.5$ eV (V_0^V is the vacuum-referenced inner potential) for our final-state band, reasonably consistent with the value determined from LEED studies[38] of Cu(001) ($V_0^V = -13.5$ eV). In contrast to several previous studies (see, e.g., Ref. 14), this Cu(211) quasi-free electron final-state dispersion relation was used without modification.

In Fig. 7, we show a comparison of our empirically derived valence-band positions (symbols) with the interpolated dispersion relations (lines) for all six valence bands along [211]. The arrows at E_F indicate $\vec{k}$ values for which A_4' intersects the Fermi surface (from de Haas-van Alphen data[39]). The empirical bands in Fig. 7 represent the combined data of (I) and (II) (Figs. 3 and 4). If a peak appeared in both orientations, the mean value was used to determine the band

position. The points in Fig. 7 were positioned in the standard way[30] by determining $\vec{k}_i$ from the final-state band highlighted in Fig. 6. Then, for each valence band, the points were fitted to a smooth curve, yielding empirical dispersion relations.

Considering both the complexity of the Cu(211) EDCs and the possible inaccuracies associated with the interpolation scheme calculation,[32] the theoretical and experimental bands generally agree quite well and both agree with the Fermi surface data.[39] The only feature in the EDCs that does not appear to arise from direct transitions is a weak shoulder at $E^F = -2.30 \pm 0.02$ eV in the spectra for 9 eV $\leq h\nu \leq$ 16 eV. It is reasonable to attribute this nondispersion feature to the d-band edge in the density of states. A similar feature was noted in silver,[6] gold,[8] and platinum[8] ARNP spectra.

We can describe the "agreement" between experiment and interpolation theory quantitatively by calculating $\Delta E = E^F(\text{expt.}) - E^F(\text{int.})$ for each energy level determined in this investigation, where $E^F(\text{int.})$ is the interpolated energy position. The results are listed in Table II, along with similar (theoretical) numbers reported by Hodges, et al.[32] for a general comparison of interpolated Cu bands with Burdick's[34] APW calculation. The theoretical ΔE values represent the general limitations of the interpolation method and thus are lower bounds on the size of ΔE values that might reasonably be expected for these Cu(211) studies. Conversely, experimentally derived ΔE values that are smaller than

those of Hodges, et al.[32] are not meaningful. By this criterion, the differences between the interpolated and experimental band structures are negligible for all bands except A_1' and A_4'. However, there are no gross deviations of the experimentally determined bands from those generated by the interpolation procedure, and the deviations that do occur may very well be caused by the finite resolution of the electron energy analyzer coupled with the inability to separate overlapping spectral features properly. In general, the agreement between the experimental and interpolated bands is quite good, and this represents the most significant result of this work.

The components of the vector potential $\vec{A}$ that are parallel to M (A_z,A_y) can excite A' transitions and A_x ($\perp$M) excites A" transitions, if the polarization selection rules are obeyed in Cu(211) (see Table I). Figure 8 illustrates the effect of polarization selection rules on Cu(211) ARNP spectra, for selected photon energies. The intensities vary as expected. Finite angular acceptance of the analyzer (±3°), angular alignment (±1° in θ, ±3° in ϕ), and incomplete polarization of the radiation (> 97 percent polarized) are among the effects that contribute to the apparent violation of these rules, which takes the forms of weak photoemission from A_1" and somewhat stronger emission from A_2" in (II), where they are both forbidden because $|A_x| = 0$ (see Fig. 2). In (I), where both $|A_x|$ and $|A_z|$ are nonzero, there is no A_4' peak except at higher photon energies, and A_1" typically dominates over A_2' and A_3'. In order to understand in detail these intensity

variations, one must know the electromagnetic field as it passes through the vacuum-solid interface[40] and the transition matrix elements. Smith, et al.[41] have discussed these effects in the ARP polarization studies of Cu(111) by Knapp, et al.[2]

It is interesting to compare EDCs for different θ_A. In Fig. 9, spectra at $h\nu = 17$ eV are shown for both orientations (I and II) and $\theta_A = 10°$, 30°, and 40°, corresponding to different electric field strengths normal and parallel to the sample surface. For (II), the spectra are normalized to the intensity of $(A_2' + A_3')$ (this is essentially A_2' at this energy), and (I) EDCs are normalized to the A_1'' intensity. Generally, only changes in relative peak intensities are induced by varying θ_A at all photon energies studied. New peak structures are <u>not</u> observed. In (II), $|A_x| = 0$; thus, the relative intensities of the four A' peaks in (II) [A_4', $(A_3' + A_2')$, and A_1'] do not change significantly with θ_A. However, it was noted above that residual experimental misalignment effectively leads to $|A_x| \gtrsim 0$. Therefore, decreasing θ_A in (II) suppresses the residual $|A_x|$ component in a manner similar (I), accounting for the observed attenuation of A_2'' intensity in (II).

Previous experimental and theoretical work on low-index faces[17,24,25] showed evidence for unusual behavior in ARP when the excitation energy placed photoelectrons into bulk conduction-band gaps. The main feature supporting this is a "lack of dispersion" of the initial-state bands,[25] arising because the $\vec{k}$ vector of the photoelectron is imaginary in the gap, thereby allowing only states at

the surface to be excited.[17,24] Because $|\vec{k}_{\parallel}| = 0$ in normal emission, band-gap photoemission corresponds to photoexcitation from $\bar{\Gamma}$, independent of photon energy. Hence, sweeping the photon energy resulted in direct transitions with concomitant valence-band dispersion as $\vec{k}_{\perp}$ was varied across the zone, until the gap was reached.[25] However, bulk conduction-band gaps along high symmetry directions invariably occur at Γ and/or zone boundaries, and it could be argued equally well that the lack of dispersion is simply a consequence of $v_g \sim 0$ for the initial-state bands. Additionally, lack of dispersion in d bands is not necessarily indicative of band-gap photoemission, because they are already reasonably flat.

As a consequence of low symmetry, the conduction-band gap between A_5' and A_6' in Cu[211] occurs away from the zone boundary, where initial-state s and s-p bands (A_1' and A_4', respectively) have large group velocities. The experimental dispersion relations in Fig. 7 show that there is no evidence for the band-gap photoemission process discussed previously. The portion of the band structure expected to be affected by the bulk band gap is enclosed within the vertical dashed lines. The s and s-p bands disperse throughout the gap region, and the absolute s-p and d-band intensities show no unusual structure in the spectra for either orientation. Previous work in this laboratory on low-index faces of Ag,[6] Au,[8,9] and Pt[8,14] also showed initial-state dispersion at photon energies for which the final states should be in a conduction-band gap, but the present Cu(211) work is by far the most convincing evidence for this,

because of the large slope in the A_1' and A_4' bands away from the zone boundary. Furthermore, Fig. 7 shows that d-band dispersion in the gap region is minimal in both theory (interpolated bands) and experiment, indicating that a dispersionless d band is not sufficient evidence for a band-gap photoemission process.

The apparent lack of band-gap photoemission leads directly to a discussion of the final-state band structure in ARP and the success of the single-plane-wave approximation for its dispersion relation. It has been shown that the finite lifetime of the photoelectron (which is relatively short in Cu at these energies[2]) introduces an imaginary component to its $\vec{k}$ vector regardless of its position in the zone,[42] and that the effect of this momentum broadening is essentially to bridge the gaps in the band structure, giving rise to more free-electron-like conduction bands.[42,43] Damping attenuates the interaction between the photoelectrons and the periodic lattice potential[43] and, since band gaps arise essentially from Bragg scattering, it is not surprising that damping closes these gaps. Strictly speaking, all of this points to the inadequacy of the one-electron band-structure picture in describing photoelectron dispersion relations.[44]

IV. SUMMARY AND CONCLUSIONS

We have presented results of normal emission ARP studies using variable-energy synchrotron radiation for the stepped Cu(211) face. The photoemission process is similar to low-Miller-index faces of

copper.[1,2,4] All peak structures in te EDCs, except for a previously observed DOS feature at the leading edge of the 3d bands and the s-p plateau, are shown to derive from nearly $\vec{k}$-conserving direct transitions along the [211] direction in k-space. The presence of the stepped surface does not introduce any other spectral features, although part of the photoemission intensity in various peaks (particular A_2' in orientation II) may arise from DOS photoemission. Excellent agreement between peak-energy positions and bulk-initial state dispersion relations is obtained if the final-state wavefunction is assumed to contain only one plane-wave component; i.e., no secondary Mahan emission features were found. This agreement with the interpolated bulk bands suggests that any photoelectron refraction effects associated with non-normal emission, i.e., from step and/or terrace directions, are negligible in this case. In consonance with previous work,[5,30] a quasi-free-electron parabolic final-state dispersion relation was used successfully, even at energies corresponding to symmetry band gaps near the zone boundary. The top and bottom valence bands, A_4' and A_1', are shown to disperse even when the final state falls in these gap regions, suggesting that the one-electron bulk band-gap picture is not applicable to the description of photoelectron conduction-band structure. Finally, radiation polarization selection rules are observed to play an important role in determining relative peak intensities. This is demonstrated in a particularly straightforward manner with Cu(211) because there are only two irreducible

representations (A' and A") for eigenstates along the [211] direction. In fact, polarization selection greatly reduces the problem of determining individual band empirical dispersion relations along the complicated [211] direction.

These studies suggest that the stepped structure of the Cu(211) surface does not significantly perturb its bulk-like electronic structure, a result which was anticipated in previous work.[20,45] In contrast to this, it would be interesting to investigate the valence-band structure properties of stepped crystal faces of the catalytically active Group VIII metals, particularly in light of recent Pt(100)-(5x1) results,[14] which showed large DOS contributions to the normal emission EDCs for the reconstructed surface.

Based on these Cu(211) results, we conclude that bulk valence-band structure determination can be applied to low-symmetry directions in a manner analogous to the (111), (100), and (110) faces, thereby alleviating the necessity for crystal faces with a specific high-symmetry orientation. This has implications for band-structure studies of more complicated materials, where it may not be possible to obtain high-symmetry faces.

Finally, to summarize the major results of this work: (1) it is possible to determine experimental valence-band dispersion relations for non-low-index directions; (2) valence-band dispersion relations for stepped Cu(211) show excellent agreement with bulk valence bands interpolated along the [211] direction; and (3) the quasi-free electron model describes photoelectron dispersion relations satisfactorily for photoemission from Cu(211).

ACKNOWLEDGMENTS

We wish to thank K. A. Mills and J. G. Tobin for assistance in carrying out some of the photoemission measurements, and Mrs. Winifred Heppler for assisting in the preparation of the copper crystal. In addition, we acknowledge M. G. Mason for many stimulating discussions.

This work was supported by the Director, Office of Energy Research, Office of Basic Energy Sciences, Chemical Sciences Division of the U.S. Department of Energy under Contract No. DE-AC03-76SF00098. It was performed at the Stanford Synchrotron Radiation Laboratory, which is supported by the Department of Energy, Office of Basic Energy Sciences and the National Science Foundation, Division of Materials Research.

REFERENCES

1. J. Stöhr, P. S. Wehner, R. S. Williams, G. Apai, and D. A. Shirley, Phys. Rev. B 17, 587 (1978); D. A. Shirley, J. Stöhr, P. S. Wehner, R. S. Williams, and G. Apai, Physica Scripta 16, 398 (1977).

2. J. A. Knapp, F. J. Himpsel, and D. E. Eastman, Phys. Rev. B 19, 4952 (1979).

3. P. O. Nilsson and L. Ilver, Solid State Commun. 17, 667 (1975); L. Ilver and P. O. Nilsson, Solid State Commun. 18, 677 (1976).

4. P. Thiry, D. Chandesris, J. Lecante, C. Guillot, R. Pinchaux, and Y. Petroff, Phys. Rev. Lett. 43, 82 (1979).

5. Z. Hussain, S. Kono, L.-G. Petersson, C. S. Fadley, and L. F. Wagner, Phys. Rev. B 23, 724 (1981), and references therein.

6. P. S. Wehner, R. S. Williams, S. D. Kevan, D. Denley, and D. A. Shirley, Phys. Rev. B 19, 6164 (1979), and references therein; K. A. Mills, M. G. Mason, R. F. Davis, R. Watson, G. Thornton, J. G. Tobin, Z. Hussain, E. Umbach and D. A. Shirley, to be published.

7. G. V. Hansson and S. A. Flodström, Phys. Rev. B 17, 473 (1978).

8. K. A. Mills, R. F. Davis, S. D. Kevan, G. Thornton, and D. A. Shirley, Phys. Rev. B 22, 581 (1980).

9. R. F. Davis, M. G. Mason, Z. Hussain, J. G. Tobin, L. E. Klebanoff, and D. A. Shirley, to be published.

10. P. Heimann, H. Miosga, and H. Neddermeyer, Solid State Commun. 29, 463 (1979).

11. G. V. Hansson and S. A. Flodström, Phys. Rev. B 18, 1572 (1978).

12. D. E. Eastman, F. J. Himpsel, and J. A. Knapp, Phys. Rev. Lett. 40, 1514 (1978); F. J. Himpsel, J. A. Knapp, and D. E. Eastman, Phys. Rev. B 19, 2919 (1979).

13. F. J. Himpsel and D. E. Eastman, Phys. Rev. B 18, 5236 (1978).

14. G. Thornton, R. F. Davis, K. A. Mills, and D. A. Shirley, Solid State Commun. 34, 87 (1980).

15. J. F. van der Veen, F. J. Himpsel, and D. E. Eastman, Phys. Rev. B 22, 4226 (1980).

16. R. F. Davis, K. A. Mills, G. Thornton, S. D. Kevan, and D. A. Shirley, VI International Conference on Vacuum Ultraviolet Radiation Physics (Charlottesville, VA, 1980), Vol. I, pp. 1-3.

17. B. Feuerbacher and R. F. Willis, J. Phys. C 9, 169 (1976).

18. See e.g., Gabor A. Somorjai, Chemistry in two Dimensions: Surfaces (Cornell University, Ithaca, NY, 1981), Chapter 4.

19. G. A. Somorjai, Adv. Catal. 26, 1 (1977); D. W. Blakely and G. A. Somorjai, J. Catal. 42, 181 (1976).

20. R. S. Williams, P. S. Wehner, S. D. Kevan, R. F. Davis, and D. A. Shirley, Phys. Rev. Lett. 41, 323 (1978).

21. K. Ždánský and Z. Šroubek, J. Phys. F 6, L205 (1976).

22. M. C. Desjonquères and F. Cyrot-Lackmann, Solid State Commun. 18, 1127 (1976).

23. Y. W. Tsang and L. M. Falicov, J. Phys. C 9, 51 (1976).

24. Peter J. Feibelman and D. E. Eastman, Phys. Rev. B 10, 4932 (1974); F. J. Himpsel, Appl. Opt. 19, 3964 (1980).

25. E. Dietz and F. J. Himpsel, Solid State Commun. 30, 235 (1979).

26. We used a solution of sodium 2-mercaptobenzimidazole-5-sulfonate and polyethylene glycol 400 in HCl; see J. S. Ahearn, J. P. Monaghan, and J. W. Mitchell, Rev. Sci. Instrum. 41, 1853 (1970).

27. B. Lang, R. Joyner, and G. A. Somorjai, Surf. Sci. 30, 440 (1972); 454 (1972).

28. S. D. Kevan and D. A. Shirley, Phys. Rev. B 22, 542 (1980).

29. G. D. Mahan, Phys. Rev. B 2, 4334 (1970).

30. See e.g., R. S. Williams, P. S. Wehner, J. Stöhr, and D. A. Shirley, Surf. Sci. 75, 215 (1978); Refs. 1, 6, 8, 9, 14, and 16.

31. The d-band interpolation scheme of N. V. Smith has been described and applied in a series of publications. Those most relevant to this paper are N. V. Smith and L. F. Mattheiss, Phys. Rev. B9, 1341 (1974) and N. V. Smith, Phys. Rev. B19, 5019 (1979).

32. L. Hodges, H. Ehrenreich, and N. D. Lang, Phys. Rev. 152, 505 (1966).

33. J. F. Janak, A. R. Williams, and V. L. Moruzzi, Phys. Rev. B 11, 1522 (1975).

34. Glenn A. Burdick, Phys. Rev. 129, 138 (1963).

35. J. Hermanson, Solid State Commun. 22, 9 (1977).

36. F. J. Himpsel, Appl. Opt. 19, 3964 (1980), and references therein.

37. P. O. Gartland, S. Berge, and B. J. Slagsvold, Physica Norvegica 7, 39 (1973).

38. S. Andersson, Surf. Sci. 18, 325 (1969).

39. M. R. Halse, Phil. Trans. Roy. Soc. A 265, 507 (1969).

40. J. A. Stratton, Electromagnetic Theory (McGraw-Hill, New York: 1941), Chapter IX.

41. N. V. Smith, R. L. Benbow, and Z. Hurych, Phys. Rev. B21, 4331 (1980).

42. J. B. Pendry, Surf. Sci. 57, 679 (1979); Low Energy Electron Diffraction (Academic Press, New York: 1974).

43. P. O. Nilsson and N. Dahlbäck, Solid State Commun. 29, 303 (1979).

44. P. O. Nilsson, J. Kanski, and C. G. Larsson, Solid State Commun. 36, 111 (1980).

45. G. S. Painter, P. J. Hennings, and R. O. Jones, J. Phys. C8, L199 (1975).

Table I. Polarization selection rules for normal photoemission from (211) faces of FCC crystals.[a]

Coordinate Axes			Irreducible Representations	Final State Symmetry	Allowed Initial Symmetries		
x	y	z			A_x	A_y	A_z
$[01\bar{1}]$	$[\bar{1}11]$	[211]	A' A"[b]	A'	A"	A'	A'

[a]The photoelectron propagation direction defines the z-axis in each case.

[b]Since the [211] axis in momentum space has no special symmetry designation, the symbols A' and A" chosen to represent the even and odd states, respectively, are those for the usual C_s symmetry classification.

Table II. Deviations between experimental and theoretical valence bands along [211] in copper.

Deviation Parameter,	Magnitude for Valence Bands Along [211] (eV)						Overall Theoretical
ΔE[a]	A_1'	A_2'	A_3'	A_1''	A_2''	A_4'	ΔE[b]
$\overline{\Delta E}$	0.11	0.04	0.06	0.01	0.06	0.20	0.09
ΔE_{rms}[c]	0.10	0.05	0.06	0.11	0.10	0.14	0.11
$\lvert\Delta E\rvert_{max}$[d]	0.29	0.10	0.11	0.24	0.21	0.32	0.37

[a] $\Delta E_i = E^F(\text{expt.}) - E^F(\text{int.})$.

[b] From comparison of interpolation scheme with Burdick's bands (Ref. 34) in copper, at 89 $\vec{k}_i$ points in the Brillouin zone; taken from Ref. 32.

[c] ΔE_{rms} = root-mean-square deviation.

[d] $|\Delta E|_{max}$ = maximum deviation.

FIGURE CAPTIONS

Fig. 1. A segment of an ideal Cu(S)-[3(111)x(100)] surface, showing three-atom terraces of (111) orientation separated by monatomic steps of (100) orientation. The $(01\bar{1})$ mirror plane cuts through the surface perpendicular to the atomic rows.

Fig. 2. Experimental geometries employed: (a) orientation I, with the plane of incidence $\perp$ to the $(01\bar{1})$ mirror plane M; (b) orientation II, with the plane of incidence $\parallel$ to M. The majority of spectra were recorded with θ_A, the angle between the surface normal $\vec{n}$ and the incident radiation vector potential $\vec{A}$, equal to 30°.

Fig. 3 Selected normal photoemission spectra for Cu(211) with photon energies in the range 9 eV $\leq h\nu \leq$ 32 eV and $\theta_A = 30°$. The spectra in panel (a) were collected with the orientation I geometry, while those in (b) were recorded with orientation II.

Fig. 4. Plot of experimental peak position versus photon energy for each structure in the Cu(211) EDCs for $\theta_A = 30°$: (a) orientation I; (b) orientation II. Open and filled circles designate weak and strong features, respectively, and the connecting lines have no theoretical significance. The plots are labelled with the appropriate initial states involved in direct transitions.

Fig. 5. The $(01\bar{1})$ mirror plane, showing the region of k-space in the first Brillouin zone along the [211] direction (dashed lines). The points B and D, both at the zone boundary, are separated by an Umklapp with $\vec{G} = (\bar{1},\bar{1},\bar{1})\ 2\pi/a$. The vector $\vec{k}_{DX}$, ending at a general point along the D - X line, is thus not actually in the [211] direction in the reduced zone scheme.

Fig. 6. The band structure of Cu interpolated along the [211] direction. The energy bands are symmetric about X, and the unoccupied bands are shown up to $E^F = 30$ eV. The bands are labeled by A' and A" irreducible representations. The A' symmetry final-state bands that carry photocurrent in the [211] direction are highlighted by cross hatches, with solid dots used to bridge the band-gap regions.

Fig. 7. Empirical [symbols: (•) A_1', A_2', A_4', DOS; (◇) A_3'; (○) $A_1"$; and (□) $A_2"$] and theoretical (solid lines, from interpolated bands in fig. 6) valence-band dispersion relations for Cu(211). A partial photon energy scale is indicated at E_F, and the vertical arrows are from de Haas-van Alphen data (Ref. 39). The dashed vertical lines bracket the region for which the $\vec{k}$-vectors lie in the bulk conduction-band gap.

Fig. 8. A direct comparison of photoemission spectra at selected photon energies for both orientations, with $\theta_A = 30°$, showing a strong dependence on radiation polarization orientation. The structures are labeled by the appropriate bands involved in direct transitions.

Fig. 9. A direct comparison of photoemission spectra at $h\nu = 17$ eV and various values of θ_A for both orientations. The direct-transition peak positions are indicated on the horizontal axis.

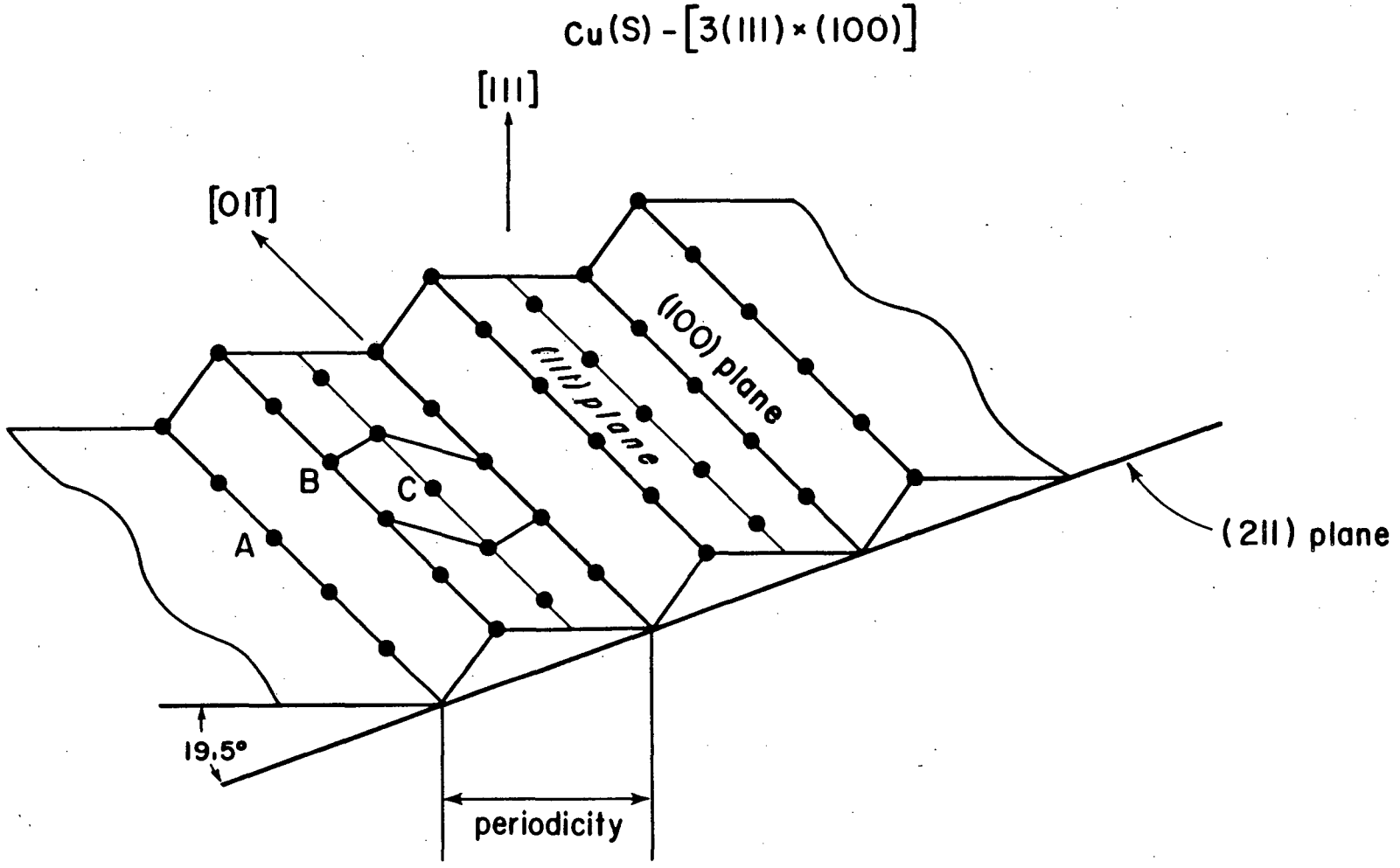
Cu(S) - [3(111) × (100)]
[111]
[01T]
(111) plane
(100) plane
A
B
C
(211) plane
19.5°
periodicity
XBL 7610-4160

Figure 1

(a) Orientation I

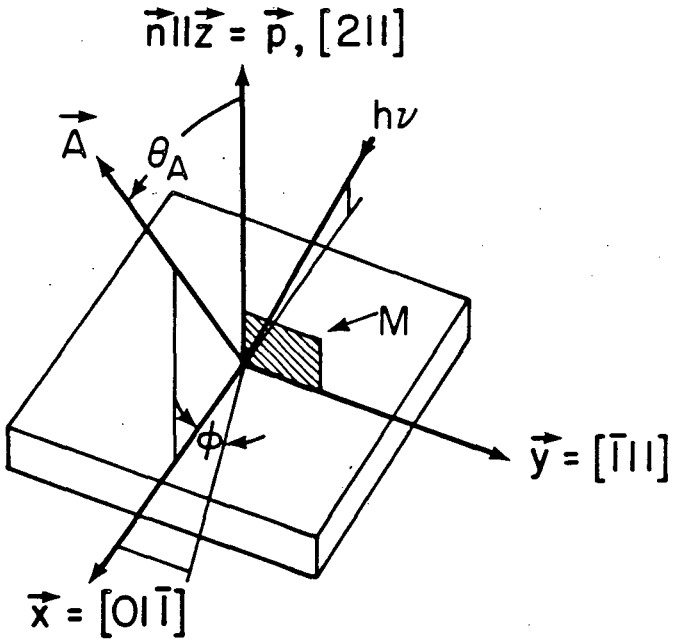

(b) Orientation II

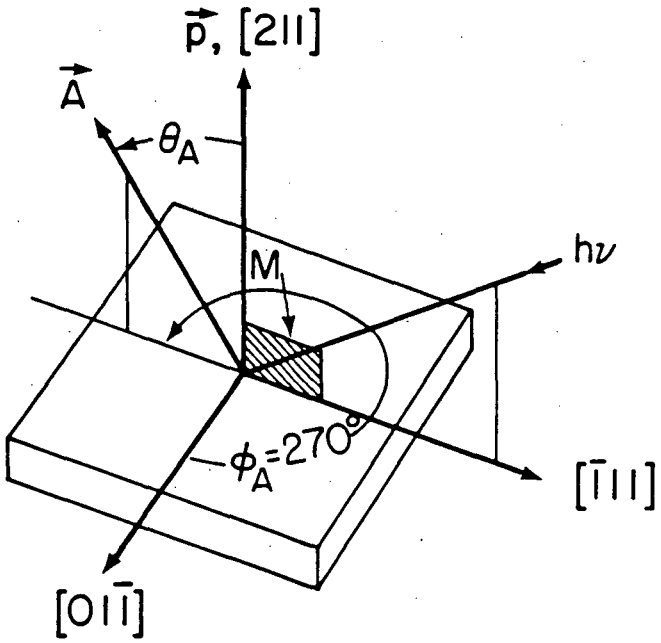

XBL 817-2379

Figure 2

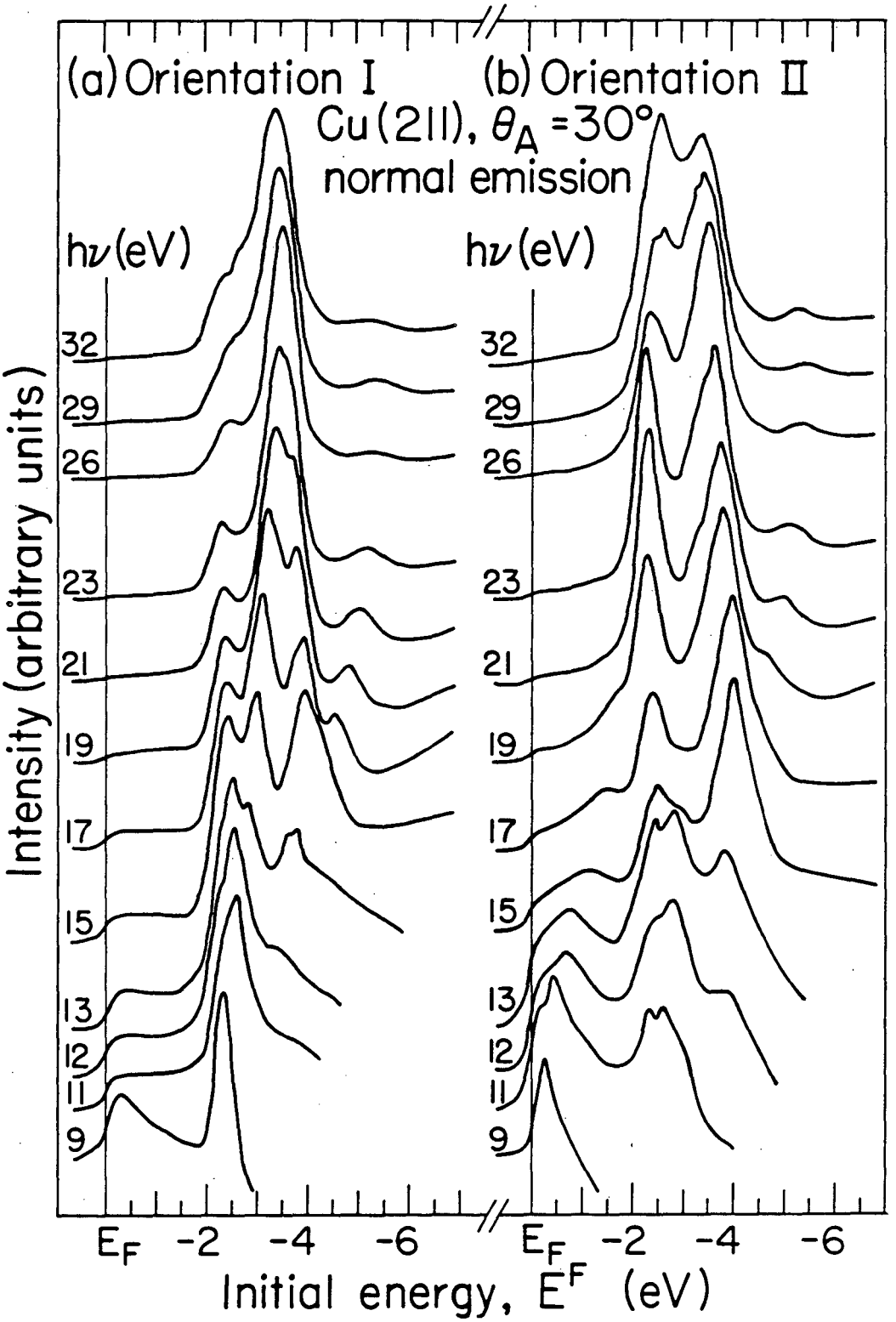
(a) Orientation I
(b) Orientation II
Cu(211), θ_A = 30°
normal emission
hν(eV)
hν(eV)
32
29
26
23
21
19
17
15
13
12
11
9
Intensity (arbitrary units)
E_F -2 -4 -6
E_F -2 -4 -6
Initial energy, E^F (eV)
XBL 817-2377

Figure 3

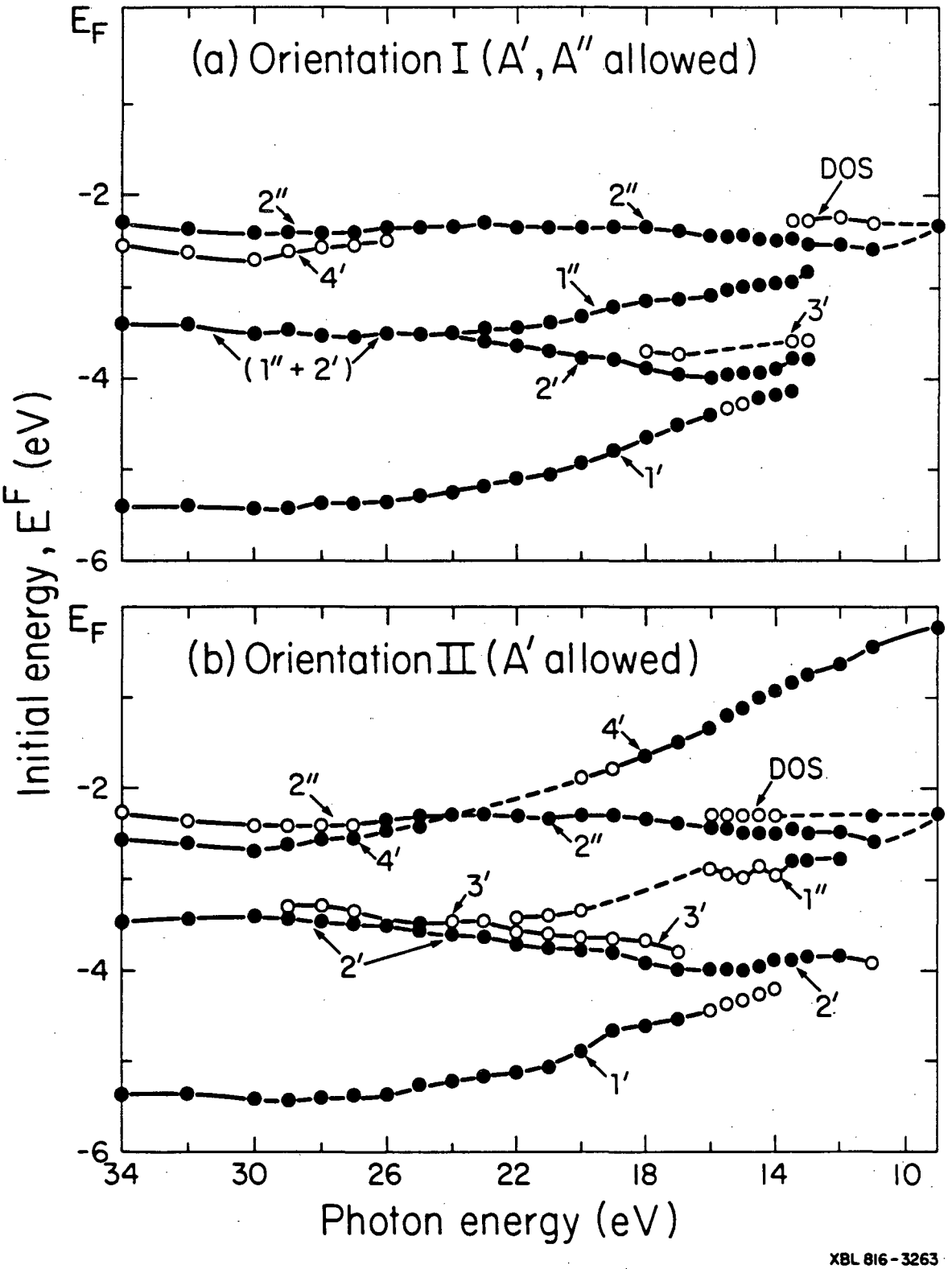
(a) Orientation I (A′, A″ allowed)
(b) Orientation II (A′ allowed)
E_F
DOS
2″
4′
1″
3′
(1″ + 2′)
2′
1′
-2
-4
-6
34
30
26
22
18
14
10
Initial energy, E^F (eV)
Photon energy (eV)
XBL 816-3263

Figure 4

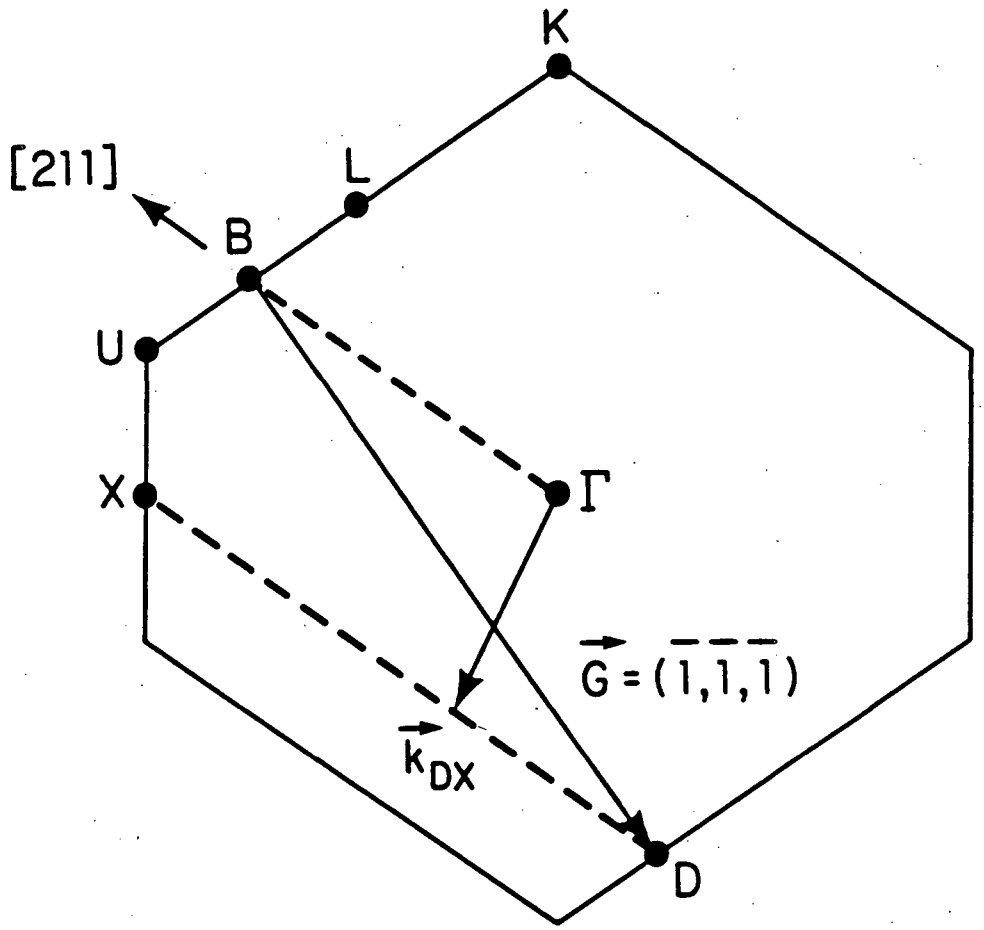
K
[211]
L
B
U
X
Γ
$\vec{G} = (\bar{1},\bar{1},\bar{1})$
$\vec{k}_{DX}$
D
(0$1\bar{1}$) projection
XBL816-3262

Figure 5

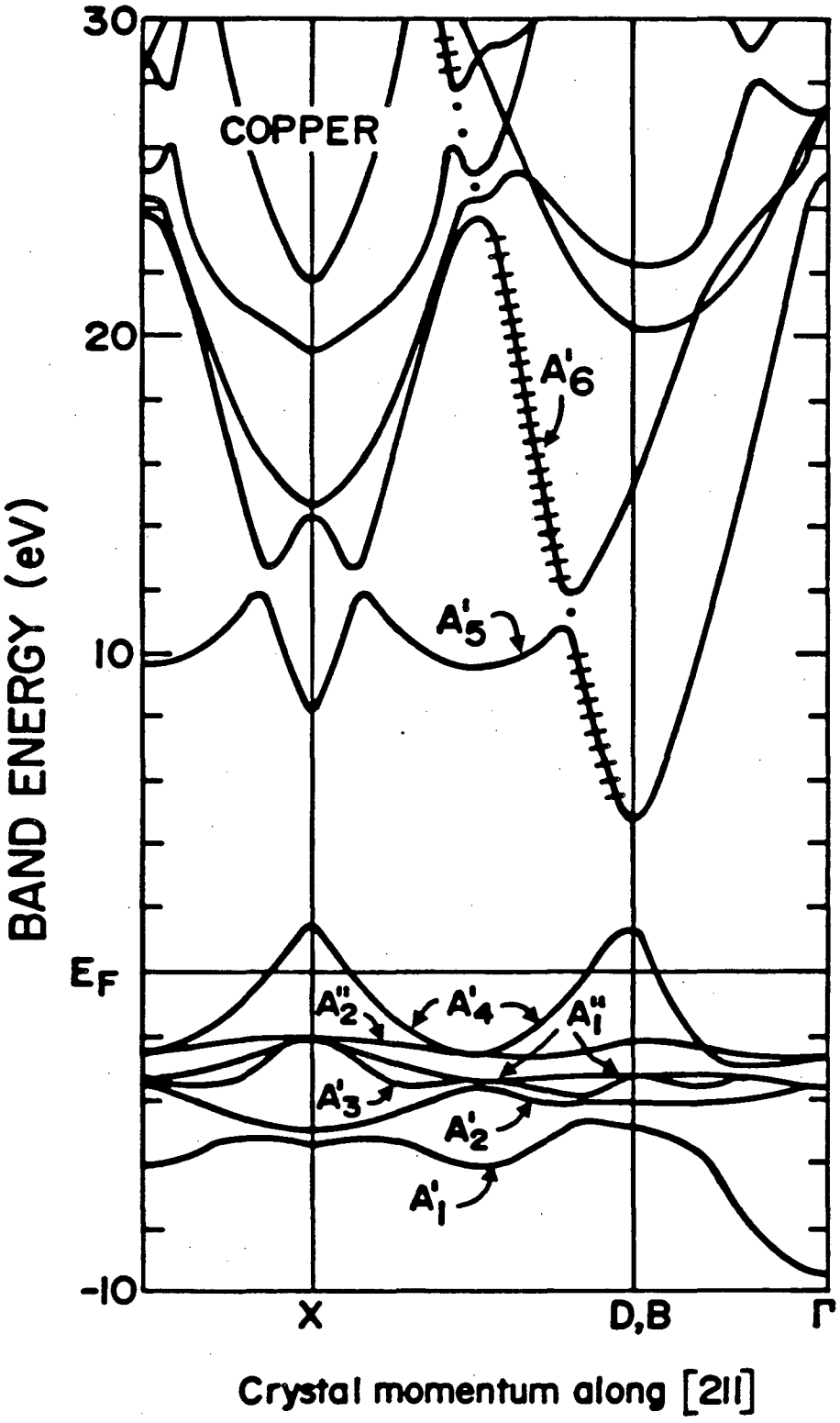
30
20
10
-10
BAND ENERGY (eV)
COPPER
A'6
A'5
E_F
A"2
A'4
A"1
A'3
A'2
A'1
X
D,B
Γ
Crystal momentum along [211]
XBL 849-3698

Figure 6

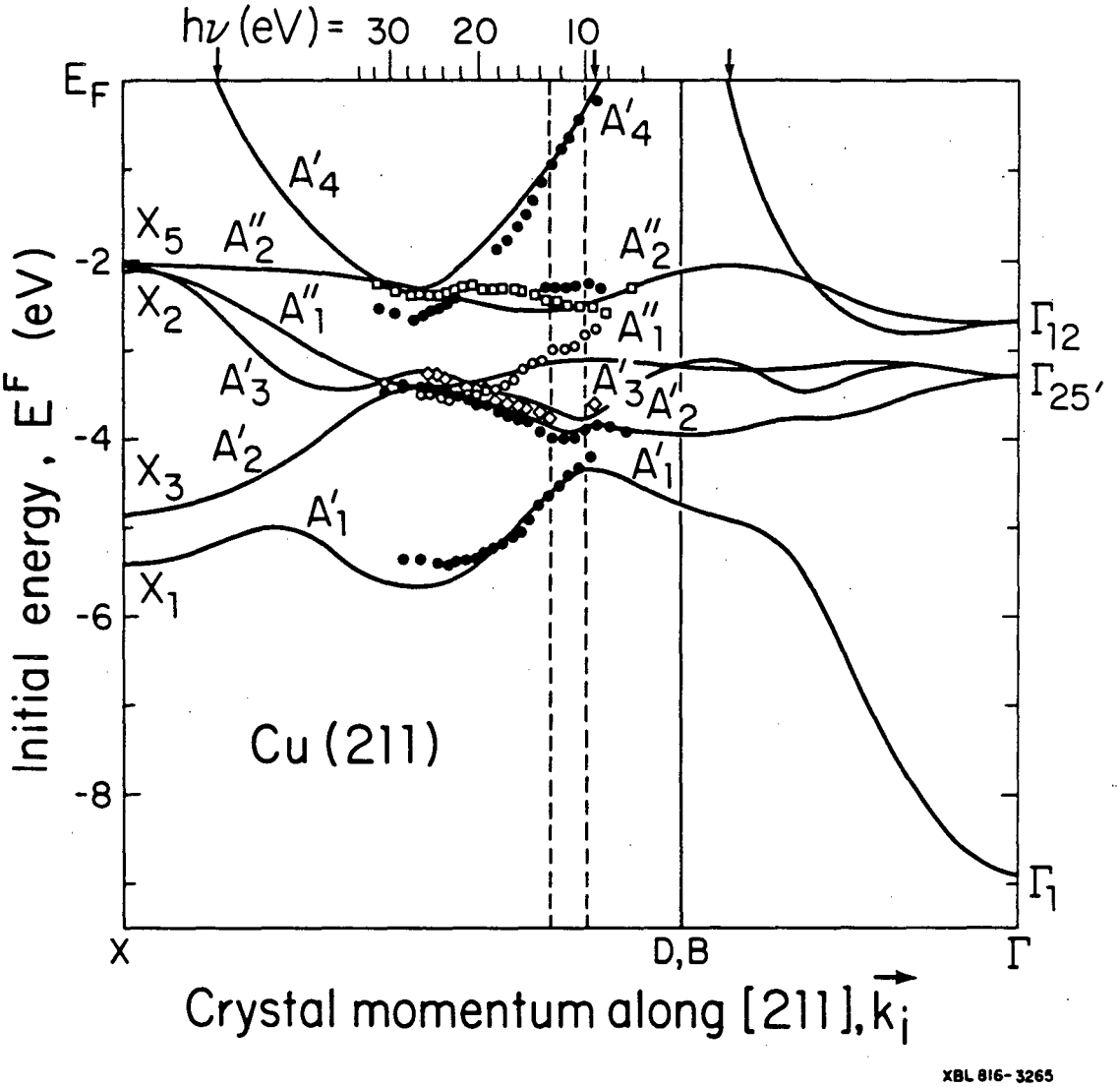
hν (eV) = 30 20 10
E_F
-2
-4
-6
-8
Initial energy, E^F (eV)
A'4
A'4
X5
A''2
A''2
X2
A''1
A''1
A'3
A'3
A'2
X3
A'2
A'1
A'1
X1
Cu (211)
Γ12
Γ25'
Γ1
X
D,B
Γ
Crystal momentum along [211], k_i
XBL 816-3265

Figure 7

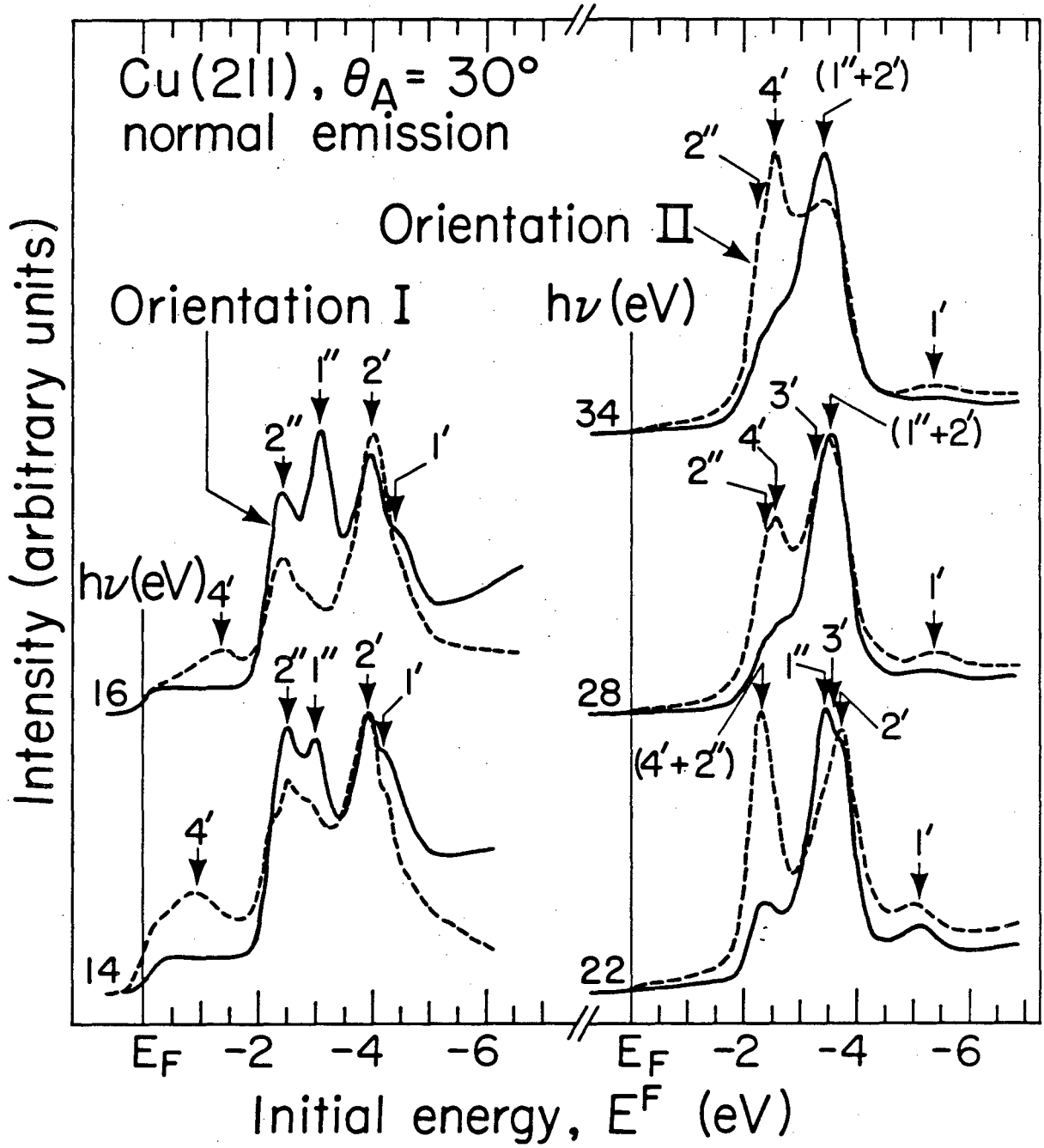

XBL 817-2378

Figure 8

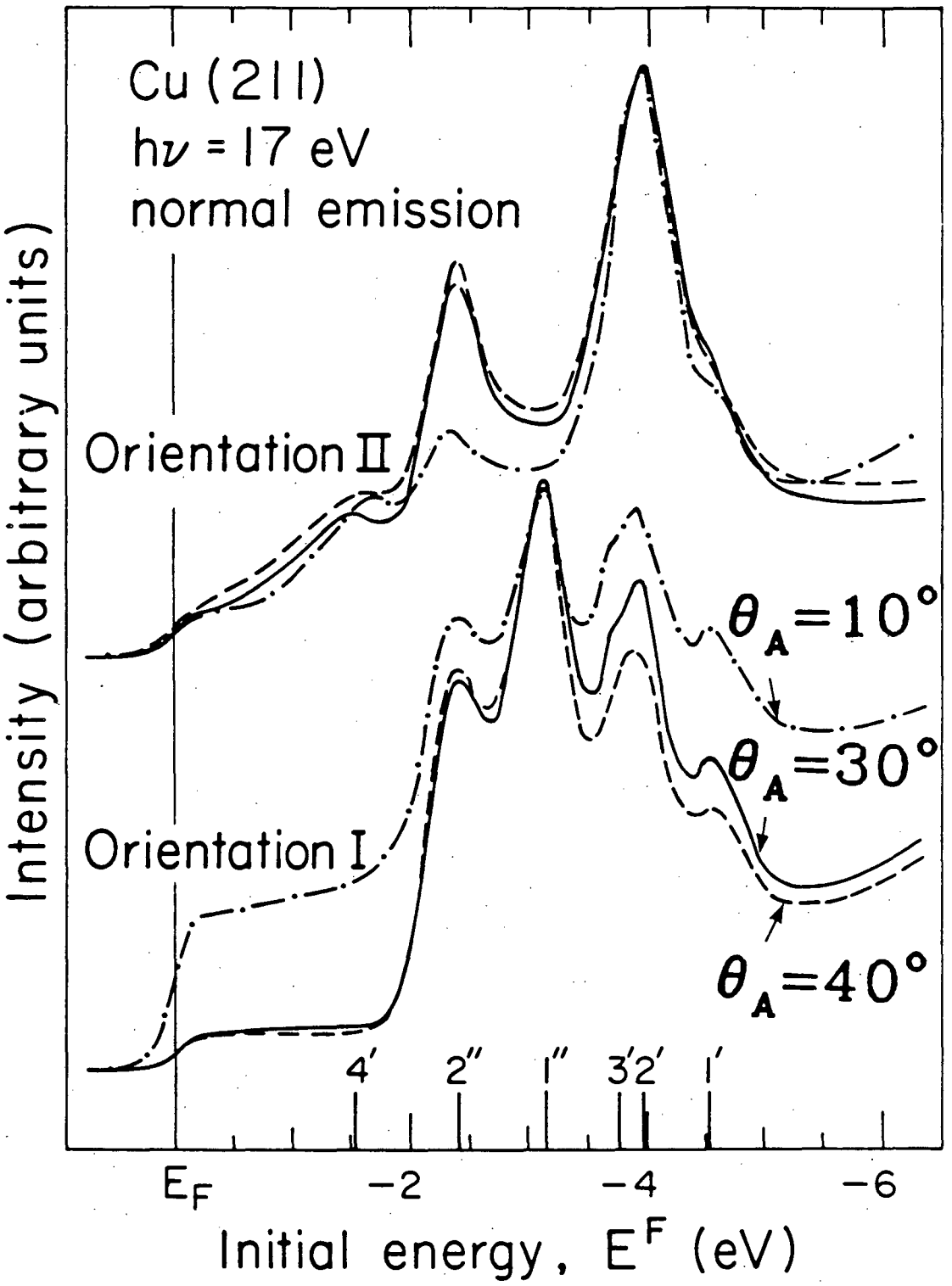

XBL 848-3624

Figure 9

TECHNICAL INFORMATION DEPARTMENT
LAWRENCE BERKELEY LABORATORY
UNIVERSITY OF CALIFORNIA
BERKELEY, CALIFORNIA 94720